Observational constraints on two-field warm inflation

Yang-Yang Wang[†] and Jian-Yang Zhu[*]
Department of Physics, Beijing Normal University, Beijing 100875, China

Xiao-Min Zhang[‡]
School of Science, Qingdao University of Technology, Qingdao 266033, China

(Received 14 January 2019; published 21 May 2019)

We study the two-field warm inflation models with a double quadratic potential and a linear temperature-dependent dissipative coefficient. We derive the evolution equation of all kinds of perturbations without assuming slow-roll approximation and obtained the curvature power spectrum at the end of inflation with a fully numerical method. Then, we compute the scalar spectral index n_s and tensor-to-scalar ratio r for several representative potentials and compare our results with observational data. At last, we use Planck data to constrain the parameters in our models. This work is a natural extension of single-field warm inflation, and the aim of this work is to present some features of multifield warm inflation using a simple two-field model.

DOI: 10.1103/PhysRevD.99.103529

I. INTRODUCTION

Inflation is widely accepted as the leading theory describing the early Universe [1–3] because it solves many long-standing puzzles of the hot big bang model, such as the horizon, flatness, and monopole problems. In addition, primordial fluctuations generated in inflation provide the seed for the large-scale structure of our Universe, and it can explain the temperature anisotropies on cosmic microwave background (CMB) naturally. In standard cold inflation, cosmological expansion and reheating are two separate periods, and we still know little about the details of reheating. The recent observational results have reached an impressive level of precision and improved the upper bound on tensor-to-scalar ratio r, so many representative models are ruled out in the standard inflationary paradigm.

Warm inflation is an alternative to standard cold inflation [4], in which the interaction between the inflaton and radiation can cause an extra dissipative term. The dissipative effects can lead to a sustainable radiation production, so the Universe can become radiation dominated without a reheating process. In warm inflation, density fluctuations come from thermal fluctuation, which is much larger than quantum fluctuations in cold inflation. Consequently, warm inflation can happen at a much smaller energy scale, and this leads to a suppressed tensor-to-scalar ratio. Many inflationary potentials excluded in cold inflation become consistent with observations again in warm inflation. There have been various studies on warm inflation [5–8], and many interesting features are explored. Although warm inflation remains an appealing alternative to standard cold inflation, realizing warm inflation in concrete models is not easy. When coupling the inflaton directly with light fields, we have to make sure that the thermal corrections to the inflaton potential are not large so that the inflaton potential remains flat and we can get sufficient e-foldings. At the same time, the dissipative effects should be strong enough to sustain a thermal bath at temperature $T > H$ during inflationary universe. In Ref. [9], the authors examined the feasibility of warm inflation from various viewpoints and showed that it was extremely difficult or perhaps even impossible to realize the idea of warm inflation. Recently, a scenario fulfilling these conditions was proposed in Ref. [10], in which the inflaton is a pseudo-Goldstone-boson coupled to a pair of fermionic fields through Yukawa interactions. In this case, the inflaton's mass gets protection from large thermal corrections due to the symmetries obeyed by the model, so the slow roll of warm inflation will not be affected. This leads to enough dissipation with only a small number of fields and a linear T dissipative coefficient.

The simplest inflationary models comprise only a single scalar degree of freedom (d.o.f.) and are sufficient to obtain predictions consistent with observational constraints. Single-field inflation may seem natural from the perspective of simplicity and economy, but the status is not certain from the perspective of the microphysical origin of inflation [11]. In fact, fundamental physics seems to predict the existence of a large number of scalar fields [12]. If the inflationary scale is not widely separated from the next

[*]Corresponding author.
zhujy@bnu.edu.cn
[†]wangyy@mail.bnu.edu.cn
[‡]zhangxm@mail.bnu.edu.cn

relevant mass scale, it is natural to expect inflationary models with more than one active scalar field. Inflation driven by multiple scalar fields has some specific features, such as large non-Gaussianity [13–15] and the presence of isocurvature perturbation [16,17], which can be narrowly constrained by the improved observational data in the future.

The content of the early Universe is usually treated as a mixture of radiation fluid and scalar fields, in which interactions between different fields and dissipative effects play an important role. Therefore, to study the dynamical and perturbation features of multicomponent cosmology and how it is constrained by observation is an important topic. One of the models including all these effects is the multifield warm inflation paradigm, in which the radiation is regarded as a perfect fluid. In this paper, we will focus on two-field warm inflation and try to reveal some features of multifield inflation by constraining our models with observational data. In our previous work [18], we showed some simple conclusions in a temperature (T)-independent dissipative coefficient γ, which is not a realistic case. Now, we extend our analysis as a next step to a linear T dissipative coefficient. In Ref. [10], it is shown that a dissipative coefficient $\gamma = C_T T$ can be realized in a little Higgs model, which puts warm inflation on a solid footing in the aspect of model building.

This work is organized as follows. In Sec. II, we introduce some basics of two-field warm inflation and derive the full set of equations describing the background dynamics and perturbations. In Sec. III, we give the main features of two-field warm inflation by numerically solving the equations obtained in Sec. II. In Sec. IV, we use the Planck data to constrain our models and give the observational constraints on model parameters. In Sec. IV, we present our conclusions.

II. BASICS OF TWO-FIELD WARM INFLATION

The two-field warm inflation dynamics is characterized by the coupled background equations of inflaton field $\phi(t)$, $\chi(t)$ and radiation density $\rho_r(t)$,

$$\begin{aligned}&\ddot{\phi} + (3H+\gamma)\dot{\phi} + V_\phi = 0,\\ &\ddot{\chi} + (3H+\gamma)\dot{\chi} + V_\chi = 0,\\ &\dot{\rho_r} + 4H\rho_r = \gamma(\dot{\phi}^2 + \dot{\chi}^2),\end{aligned} \tag{2.1}$$

where V is the inflaton potential, $V_\phi = \partial V(\phi,\chi)/\partial\phi$, $V_\chi = \partial V(\phi,\chi)/\partial\chi$, overdots represent derivatives with respect to cosmic time t, and γ is the dissipative coefficient. In the general case, γ is a function of background inflaton fields and the temperature T. For simplicity, we will use the Planck unit in the context

$$8\pi G = k_B = \hbar = c = 1,$$

where G is Newton's gravitational constant, k_B is Boltzmann's constant, $\hbar$ is the reduced Planck's constant, and c is the speed of light. In a spatially flat universe, the Friedmann equations read

$$3H^2 = \frac{1}{2}\dot{\phi}^2 + \frac{1}{2}\dot{\chi}^2 + V(\phi,\chi) + \rho_r, \tag{2.2}$$

and the slow-roll parameters are defined as

$$\epsilon = -\frac{\dot{H}}{H^2}, \qquad \eta = -\frac{\ddot{H}}{2H\dot{H}}. \tag{2.3}$$

Inflation takes place when the slow-roll conditions $\epsilon < 1$ and $|\eta| < 1$ are satisfied. In slow-roll approximation, we have

$$(3H+\gamma)\dot{\phi} + V_\phi = 0, \tag{2.4}$$

$$(3H+\gamma)\dot{\chi} + V_\chi = 0, \tag{2.5}$$

$$4H\rho_r = \gamma(\dot{\phi}^2 + \dot{\chi}^2). \tag{2.6}$$

For convenience, we define adiabatic field σ and entropy field s by making a rotation in field space, where $d\sigma$ is tangent to the background trajectory and ds is normal to it [19,20],

$$\begin{pmatrix} d\sigma \\ ds \end{pmatrix} = \begin{pmatrix} \cos\theta & \sin\theta \\ -\sin\theta & \cos\theta \end{pmatrix} \begin{pmatrix} d\phi \\ d\chi \end{pmatrix}, \tag{2.7}$$

where $\cos\theta = \frac{\dot{\phi}}{\sqrt{\dot{\phi}^2+\dot{\chi}^2}}$, $\sin\theta = \frac{\dot{\chi}}{\sqrt{\dot{\phi}^2+\dot{\chi}^2}}$. With this definition, the background equations (2.1) and (2.2) become

$$\begin{aligned}&\ddot{\sigma} + (3H+\gamma)\dot{\sigma} + V_\sigma = 0,\\ &\dot{\theta}\dot{\sigma} + V_s = 0,\\ &\dot{\rho_r} + 4H\rho_r = \gamma\dot{\sigma}^2,\\ &3H^2 = \frac{1}{2}\dot{\sigma}^2 + V + \rho_r,\end{aligned} \tag{2.8}$$

where $V_\sigma = \cos\theta V_\phi + \sin\theta V_\chi$ and $V_s = -\sin\theta V_\phi + \cos\theta V_\chi$. In this case, slow-roll parameters can be expressed by

$$\begin{aligned}&\epsilon = \epsilon_\sigma + \epsilon_r, \qquad \epsilon_\sigma = \frac{1}{2}\frac{\dot{\sigma}^2}{H^2}, \qquad \epsilon_r = \frac{2}{3}\frac{\rho_r}{H^2},\\ &\eta = \frac{\epsilon_\sigma}{\epsilon}\eta_\sigma + \frac{\epsilon_r}{\epsilon}\eta_r, \qquad \eta_\sigma = -\frac{\ddot{\sigma}}{H\dot{\sigma}}, \qquad \eta_r = -\frac{1}{2}\frac{\dot{\rho_r}}{H\rho_r}.\end{aligned} \tag{2.9}$$

To study the evolution of perturbations, we decompose each of the fields into a spatially homogenous background

field and its perturbations, $\phi(x,t) \to \phi(t) + \delta\phi(x,t)$, and $\chi(x,t) \to \chi(t) + \delta\chi(x,t)$. Similarly, it is convenient to decompose the field perturbation into an adiabatic component $\delta\sigma$ and entropy component δs [21],

$$\begin{pmatrix} \delta\sigma \\ \delta s \end{pmatrix} = \begin{pmatrix} \cos\theta \sin\theta \\ -\sin\theta \cos\theta \end{pmatrix} \begin{pmatrix} \delta\phi \\ \delta\chi \end{pmatrix}. \tag{2.10}$$

The line element of the Friedmann-Robertson-Walker metric is given by

$$ds^2 = -(1+2A)dt^2 + 2a\partial_i B dx^i dt + a^2((1-2\psi)\delta_{ij} + 2\partial_i\partial_j E)dx^i dx^j. \tag{2.11}$$

In warm inflation, we have to take into account the perturbations resulting from both the inflation field and radiation. Therefore, the total gauge-invariant comoving curvature perturbation can be split into two parts [22–24],

$$\mathcal{R} = \frac{\epsilon_\sigma}{\epsilon}\mathcal{R}_\sigma + \frac{\epsilon_r}{\epsilon}\mathcal{R}_r, \tag{2.12}$$

where $\mathcal{R}_\sigma = \psi + H\frac{\delta\sigma}{\dot\sigma}$, $\mathcal{R}_r = \psi - aH(B+\delta u)$, and δu is the scalar velocity potential of the radiation fluid. For convenience, we also define the isocurvature perturbation $\mathcal{S} = H\frac{\delta s}{\dot\sigma}$. The power spectrum of comoving curvature $\mathcal{R}$ perturbation is given by

$$\mathcal{P}_\mathcal{R} = \frac{k^3}{2\pi^2}\langle\mathcal{R}^2\rangle, \tag{2.13}$$

and the power spectrum of inflaton perturbation $\mathcal{R}_\sigma$, radiation perturbation $\mathcal{R}_r$, and isocurvature perturbation $\mathcal{S}$ are [25]

$$\mathcal{P}_\sigma = \frac{k^3}{2\pi^2}\langle\mathcal{R}_\sigma^2\rangle, \qquad \mathcal{P}_r = \frac{k^3}{2\pi^2}\langle\mathcal{R}_r^2\rangle, \qquad \mathcal{P}_\mathcal{S} = \frac{k^3}{2\pi^2}\langle\mathcal{S}^2\rangle, \tag{2.14}$$

where k denotes the comoving wave number. In warm inflation, density perturbations mainly arise from thermal noise [26]. On small scales ($k \gg aH$), the metric fluctuations have little effects [27,28], so inflaton fluctuations $\delta\varphi_I$ ($\delta\varphi_I = \delta\phi, \delta\chi$) are described by a Langevin equation [29],

$$\delta\ddot\varphi_I(k,t) + (3H+\gamma)\delta\dot\varphi_I(k,t) + \frac{k^2}{a^2}\delta\varphi_I = \xi_I(k,t), \tag{2.15}$$

where $\xi_I(k,t)$ is a white-noise term and different components of $\xi_I(k,t)$ are independent of each other. In this case, there is no coupling between different components of inflaton perturbations before horizon crossing, which is a common assumption in standard multifield inflation. In the high-temperature limit, the noise source is Markovian,

$$\langle\xi_I(k,t)\xi_J(-k',t')\rangle = 2\gamma T a^{-3}(2\pi)^3\delta_{IJ}\delta^3(k-k')\delta(t-t'), \tag{2.16}$$

where T denotes the temperature and a is the scale factor. The relationship between radiation energy density ρ_r and T is $\rho_r = \frac{\pi^2}{30}g_* T^4$, where g_* is the effective particle number of radiation fluid [30]. We will take $g_* = 228.75$ in the following numerical calculation, which is the number of d.o.f. for the minimal supersymmetric Standard Model [31,32]. After horizon crossing, the effects of thermal noise are suppressed, while the metric perturbation come to play an important role [33]. In previous studies, the perturbations in subhorizon and superhorizon scales are often treated separately for simplicity. The power spectrum in warm inflation has been studied in many previous works [34–36], and a general expression for amplitude of the inflaton power spectrum is given by [37]

$$\mathcal{P}^*_{\delta\sigma} = \left(\frac{H_*}{2\pi}\right)^2\left(\frac{T_*}{H_*}\frac{2\pi Q_*}{\sqrt{1+4\pi Q_*/3}} + 1 + 2n_*\right)G(Q_*), \tag{2.17}$$

where a subscript * denotes variables evaluated at horizon crossing, $Q = \gamma/(3H)$ is the dissipative ratio, and $n_* = 1/(e^{H_*/T_*}-1)$ is the statistical distribution of inflaton fluctuations at horizon crossing [38]. The function $G(Q_*)$ represents the growth of $\mathcal{P}_\mathcal{R}$ due to the coupling between inflaton fluctuations and radiation fluctuations, and this growing function can only be determined by solving the perturbation equations numerically.

When performing numerical calculations, it is more convenient to take e-foldings N ($dN = Hdt$) as the time variable. To get a full picture of the evolution of perturbations, we take into account all kinds of perturbations in two-field warm inflation and give the evolution equation of $\mathcal{R}_\sigma$, $\mathcal{R}_r$, and δs beyond slow-roll approximation (see the Appendix A for more details),

$$\begin{aligned}
&\mathcal{R}_\sigma'' + (3+3Q+\epsilon_r+\epsilon_\sigma-2\eta_\sigma)\mathcal{R}_\sigma' + (z^2 - 2\lambda_\theta{}^2\epsilon_\sigma - 9Q + 2(1+\epsilon_r-\eta_\sigma)\epsilon_r + Q(3\epsilon_r - 11\epsilon_\sigma + 6\eta_r))\mathcal{R}_\sigma \\
&\quad = -(3Q+2\epsilon_r)\mathcal{R}_r' + (-9Q + 2(1+\epsilon_r-\eta_\sigma)\epsilon_r + Q(3\epsilon_r - 11\epsilon_\sigma + 6\eta_r))\mathcal{R}_r \\
&\qquad + 2\lambda_\theta\delta s' + 2(\lambda_\theta(3+3Q-\epsilon_r-\eta_\sigma) + \lambda_{\theta\theta})\delta s + \frac{z^{3/2}k^{-3/2}}{\sqrt{2\epsilon_\sigma}}\xi_\sigma,
\end{aligned} \tag{2.18}$$

$$\mathcal{R}_r'' + \left(6 + \epsilon_r + \epsilon_\sigma - \frac{7}{2}\eta_r\right)\mathcal{R}_r' + \left(\frac{1}{3}z^2 + 9 + \frac{1}{2}(-9+\epsilon_\sigma)\eta_r + 2(4+\epsilon_\sigma - 2\eta_r)(\epsilon_r + \epsilon_\sigma - \eta_\sigma) + \left(-1 + Q + \frac{2}{3}\epsilon_r\right)\epsilon_\sigma\right)\mathcal{R}_r = \left(\frac{2}{3}\epsilon_\sigma + \frac{5}{4}(4-2\eta_r)\right)\mathcal{R}_\sigma' + \left(9 + \frac{1}{2}(-9+\epsilon_\sigma)\eta_r + 2(4+\epsilon_\sigma - 2\eta_r)(\epsilon_r + \epsilon_\sigma - \eta_\sigma) + \left(-1 + Q + \frac{2}{3}\epsilon_r\right)\epsilon_\sigma\right)\mathcal{R}_\sigma + \frac{1}{3}(-6 + 2\epsilon_\sigma + 3\eta_r)\lambda_\theta \delta s, \tag{2.19}$$

$$\delta s'' + (3 + 3Q - \epsilon_r - \epsilon_\sigma)\delta s' + \left(z^2 + \frac{V_{ss}}{H^2} - 2\lambda_\theta{}^2\epsilon_\sigma\right)\delta s = -4\lambda_\theta\epsilon_\sigma\mathcal{R}_\sigma' - 4\lambda_\theta\epsilon_\sigma\epsilon_r\mathcal{R}_\sigma + 4\lambda_\theta\epsilon_\sigma\epsilon_r\mathcal{R}_r + z^{3/2}k^{-3/2}\xi_s, \tag{2.20}$$

where a prime denotes a derivative with respect to e-folding N and $\lambda_\theta = \theta'/\sigma'$, $\lambda_{\theta\theta} = \theta''/\sigma'$. $V_{ss} = \sin^2\theta V_{\phi\phi} + \cos^2\theta V_{\chi\chi}$ is the effective mass of entropy field s, and $z = \frac{k}{aH}$. ξ_σ and ξ_s are two Gaussian white noises, and their correlation functions are

$$\langle \xi_I(k,N)\xi_J(-k',N')\rangle = 2\gamma T(2\pi)^3\delta_{IJ}\delta^{(3)}(k-k')\delta(N-N') \tag{2.21}$$

where $I, J = \sigma, s$. Similarly, using N as the time variable, we can put Eqs. (2.1) and (2.2) in the form

$$\phi'' + (3 + 3Q - \epsilon)\phi' + \frac{V_\phi}{H^2} = 0, \tag{2.22}$$

$$\chi'' + (3 + 3Q - \epsilon)\chi' + \frac{V_\chi}{H^2} = 0, \tag{2.23}$$

$$\rho_r' + 4\rho_r = 3H^2Q(\phi'^2 + \chi'^2), \tag{2.24}$$

$$\left(3 - \frac{1}{2}\phi'^2 - \frac{1}{2}\chi'^2\right)H^2 = V + \rho_r. \tag{2.25}$$

Note that the slow-roll parameters in the above equations are treated as a function of time variable N and can be determined by solving background equations (2.22)–(2.25). When dealing with multifield inflation, it is necessary to go beyond slow roll, or we will miss some important features. In this case, the numerical method is almost essential, because we can hardly find any analytic results.

III. NUMERICAL EXAMPLES

To get a picture of the dynamics and perturbations of two-field warm inflation, we apply the formalism to a simple example in this section. We use the two-field quadratic inflation as an example, in which the potential is given by [39]

$$V(\phi,\chi) = \frac{1}{2}m_\phi^2\phi^2 + \frac{1}{2}m_\chi^2\chi^2. \tag{3.1}$$

Although these two scalar fields have no direct coupling, they can interact gravitationally during inflation. We will show that even the simplest two-field warm inflation models can display interesting features, which is very different from the single-field cases. In the following calculations, we set $N = 0$ when the relevant scales cross

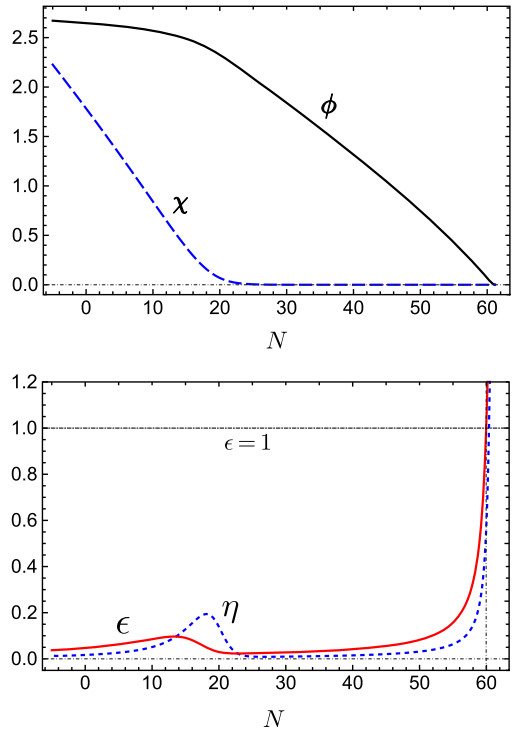

FIG. 1. The evolution of inflaton (ϕ,χ) and slow-roll parameters ϵ and η are shown against e-foldings N. In this example, we choose the initial condition $(\phi_0,\chi_0) = (2.67, 2.23)$, $C_T = 0.048$, and inflation ends at about $N = 60$ in this case. From the lower panel, we can know that when the field χ decays to zero a local extreme occurs for slow-roll parameters ϵ and η.

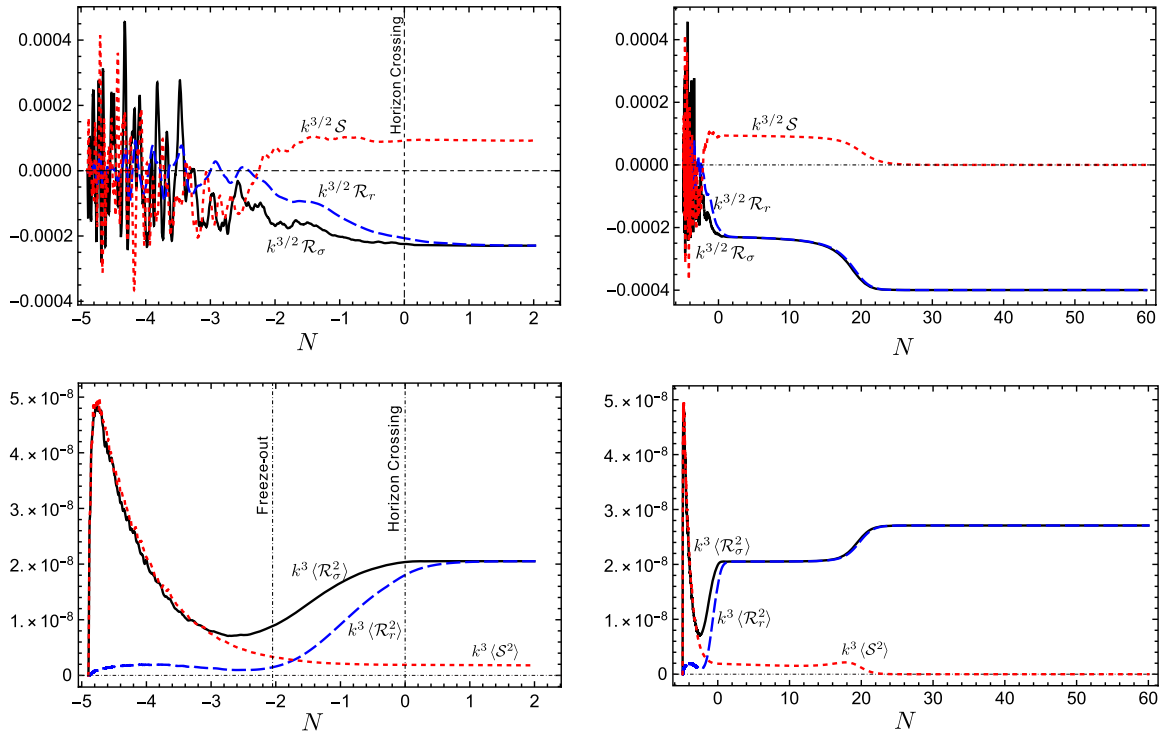

FIG. 2. The evolution of perturbations $\mathcal{R}_\sigma$, $\mathcal{R}_r$, and $\mathcal{S}$ and the power spectrum of each kind of perturbations are shown in this figure. In the top two panels, we show a single realization of the stochastic perturbation equation, and the power spectrum of each perturbation is illustrated in the lower two panels, which represent an average over 5000 runs. We zoom in to the few e-foldings around horizon crossing to given more details in the left two panels.

the Hubble horizon, and we fix $N_e = 60$ when inflation ends for definite calculation.

At the beginning of our analysis, we use a representative example to demonstrate the main features of background dynamics and perturbations of two-field warm inflation. In the example, we set $m_\phi = 2 \times 10^{-8}$, and the mass ratio $R_{\rm m} = m_\chi/m_\phi = 5$. After choosing the initial condition $(\phi_0, \chi_0) = (2.67, 2.23)$ and $C_T = 0.0483$, we can perform our numerical computation by solving the background equations (2.22)–(2.25) and stochastic perturbation equations (2.18)–(2.20). Note that, since the background dynamics will tend to the slow-roll trajectory soon, the initial values of $\dot{\phi}_*$, $\dot{\chi}_*$, and ρ_{r*} have little impact on the final results. To eliminate the influence of initial conditions of perturbations equations, we begin our numerical integration about five e-foldings before the Hubble exit. The results are shown in Figs. 1 and 2.

In warm inflation, thermal effects decrease until the fluctuations freeze out, which is determined by $k^2/a^2 \approx (3H + \gamma)H$, and the freeze-out time N_F always precedes the horizon crossing time [40]. According to Fig. 2, we know before freeze-out time the system is dominated by stochastic noise, and the initial condition of perturbations has little impact on the final results. In the period between freeze-out and horizon crossing, the power spectrum $\mathcal{P}_\sigma$ and $\mathcal{P}_r$ may get enhanced due to the coupling between perturbations of radiation and inflaton, as illustrated in the lower left panels of Fig. 2. This growing mode occurs only when $Q_* > 1$ (in the example illustrated in Fig. 2, $Q_* \approx 10$), and in the weak regime of warm inflation, this is replaced by a constant mode [41]. After horizon crossing, the power spectrum $\mathcal{P}_\mathcal{R}$ does not change for a while until the turning occurs at the background trajectory. When the background evolution trajectory changes direction, the parameter $\dot{\theta}^2$ can become large, which makes perturbations $\mathcal{R}_\sigma$ and $\mathcal{R}_r$ couple strongly with the isocurvature perturbation $\mathcal{S}$ as shown in Eqs. (2.18), (2.19), and (2.20). At this moment, $\mathcal{R}_\sigma$ and $\mathcal{R}_r$ increase obviously, while $\mathcal{S}$ decays to zero. In the following period, there is only one active scalar field, and the curvature perturbation tends to a constant value. We also know from the top two panels of Fig. 2 that $\mathcal{R}_\sigma \approx \mathcal{R}_r$ on superhorizon scales, and they evolve together until the end of inflation. Therefore, we can use $\mathcal{R}_\sigma$ to represent curvature perturbation $\mathcal{R}$ according to Eq. (2.12).

IV. CONSTRAINTS FROM OBSERVATIONAL DATA

In previous subsection, we showed the main features of background dynamics and perturbation power spectrum in two-field warm inflation, and now we turn to the

consistency with observational data. To compare with the observational data, we should get the power spectrum $\mathcal{P}_\mathcal{R}$ at the end of inflation first, and then we can obtain the spectral index n_s using the finite difference method [42],

$$n_s - 1 = \frac{d\ln \mathcal{P}_\mathcal{R}}{d\ln k}. \tag{4.1}$$

The tensor mode of perturbations is not affected by the thermal noise, so the tensor power spectrum and tensor-to-scalar ratio are given by [43]

$$\mathcal{P}_T = 8\left(\frac{H_*}{2\pi}\right)^2, \qquad r = \frac{\mathcal{P}_T}{\mathcal{P}_\mathcal{R}}. \tag{4.2}$$

There exist two methods available to compute the final $\mathcal{P}_\mathcal{R}$. The most straightforward way is the method we use in the previous section, where we perform our analysis by solving the coupled stochastic system numerically until the end of inflation. However, this is a computationally intensive way, and the calculations consume a lot of CPU time because we have to perform tens of thousands of runs to get a relatively accurate result. There exists another approach to achieve our purpose that is used more widely. We can use the analytic expression (2.17) to express $\mathcal{P}_{\delta\sigma}$ at horizon crossing, and the growing function $G(Q_*)$ can be determined by integrating the stochastic equations a few e-foldings before horizon crossing. After horizon crossing, we can use δN formalism to get the time evolution of $\mathcal{P}_\mathcal{R}$ until the end of inflation,

$$\mathcal{P}_\mathcal{R} = \mathcal{P}^*_{\delta\sigma}(N^2_{\phi_*} + N^2_{\chi_*}), \tag{4.3}$$

where $\mathcal{P}^*_{\delta\sigma}$ is the power spectrum of field perturbation $\delta\sigma$ at horizon crossing.

In the following investigation, we take four representative values of mass ratio R_m, $R_\mathrm{m} = 1$, $R_\mathrm{m} = 1.5$, $R_\mathrm{m} = 2$, and $R_\mathrm{m} = 3$ as examples. To obtain the growing function $G(Q_*)$ in Eq. (2.17) in two-field warm inflation, we carry out a numerical simulation for each value of R_m. $G(Q_*)$ and numerical results of simulations are shown in Fig. 3. According to Fig. 3, we know the function $G(Q_*)$ fits well with the numerical results.

With a given mass ratio R_m, for every set of initial conditions (ϕ_*, χ_*), we can determine the value of m_ϕ and C_T using $N_e = 60$ and observational constraints $\mathcal{P}_\mathcal{R} = 2.2 \times 10^{-9}$ at the end of inflation. And then with the value of (m_ϕ, C_T), we can obtain the spectral index and tensor-to-scalar ratio (n_s, r) with Eqs. (4.1) and (4.2). Therefore, we have a corresponding (n_s, r) for every set of initial conditions (ϕ_*, χ_*). We show the final value of spectral index n_s with initial condition (ϕ_*, χ_*) in Fig. 4. In every panel in Fig. 4, the damping strength Q_* is larger when (ϕ_*, χ_*) are near the original point (0, 0). According to the figure, we know the strong dissipative effect will render the spectrum blue tilted, which agrees with the conclusion in

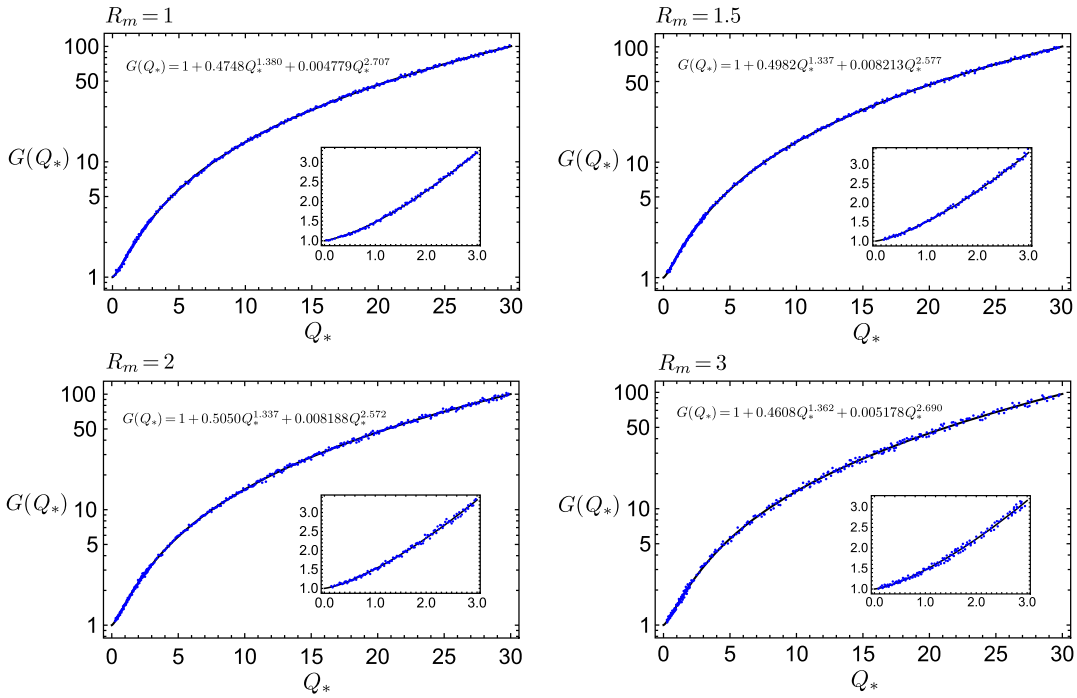

FIG. 3. The numerical results (blue dots) and analytic fitting function of $G(Q_*)$ (black line) are shown against Q_*. In general, the analytic expression $G(Q_*)$ fits well with the numerical results, and the figure shows the growing function $G(Q_*)$ is slightly different for different potentials. In the lower right part of each panel, we zoom in to give more details for small values of Q_*.

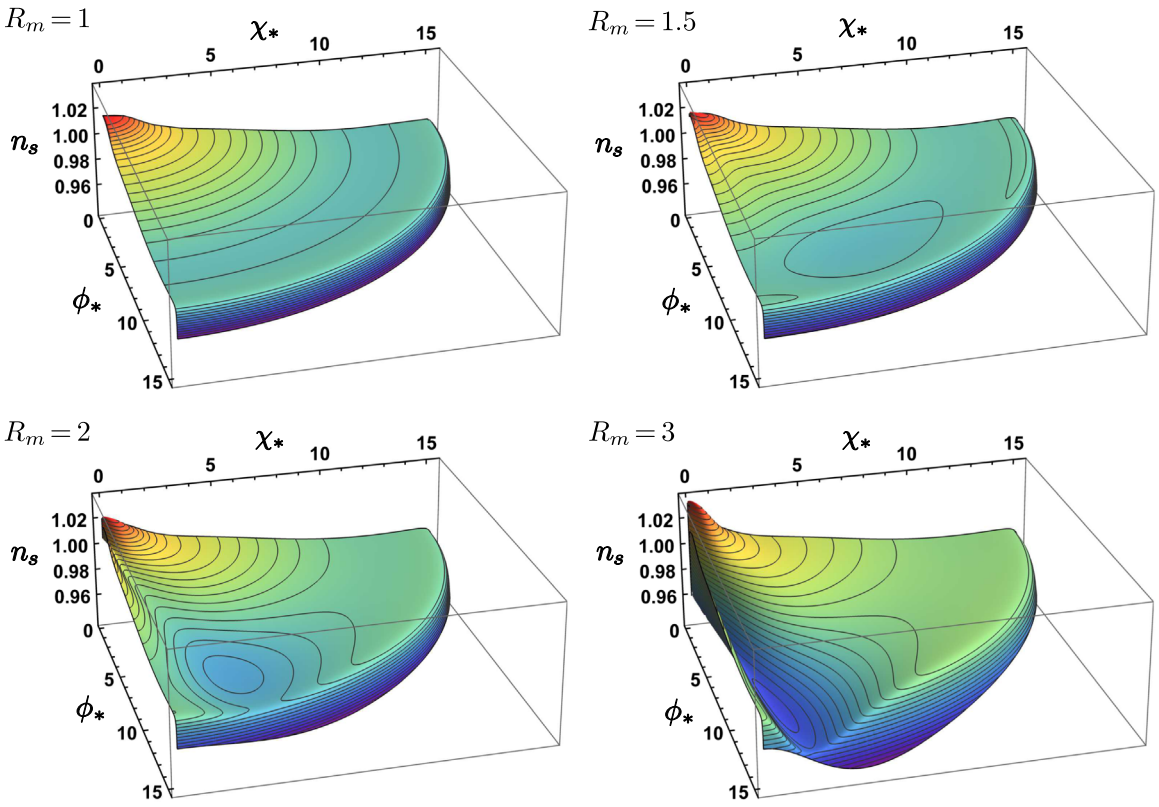

FIG. 4. The final spectral index n_s is plotted against the initial condition (ϕ_*, χ_*). In each panel, the dissipative ratio Q_* is generally larger when (ϕ_*, χ_*) are closer the original point (0, 0), and the farthest points in each direction denote $Q_* = 0$ (cold two-field inflation). The figure also shows that the dissipative effects will render the power spectrum blue tilted. Meanwhile, multifield effects will make n_s take values in a wider range.

single-field cases. In all directions, the farthest (ϕ_*, χ_*) from the original point represent the case $Q_* = 0$ (cold inflation). We also find that when $R_m = 1$ ($m_\phi = m_\chi$), n_s is the same for all the points (ϕ_*, χ_*) of the same distance from the original point. However, this property of symmetry no longer exists when $R_m \neq 1$. In fact, when $R_m = 1$, the background evolution trajectory is a straight line in field space of (ϕ, χ), so there is only 1 d.o.f., which is the same as single-field cases. In the following context, we use this case to represent an example of single-field warm inflation for comparison with other cases.

To compare our results with observational data directly, we also show our results in the (n_s, r) plane, as illustrated in Fig. 5. For each $R_{\rm m}$, we plot (n_s, r) in the same plot with the allowed contour plots of Planck data (68% and 95% C.L. results from Planck 2018 TT,TE,EE+lowE +lensing) [44]. Note that in the figure we represent $Q_* = 0$, $Q_* = 1$, and $Q = 10$ with thick black lines (the line for $Q_* = 0$ is at the top of the blue-shaded region, which represents the cold inflation cases). As described above, we can treat the $R_{\rm m} = 1$ case as a single-field warm inflation example. Comparing $R_{\rm m} = 1$ with other values of $R_{\rm m}$, we can conclude that the multifield effects will make n_s distribute in a wide range for every value of r, rather than a point. Besides, the dissipative effects have an impact on both the spectral index n_s and tensor-to-scalar ratio r, while the multifield effects have little influence on r. According to Fig. 5, in single-field cases, the strong version of warm inflation ($Q_* > 1$) is disfavored by observation because it predicts too large n_s. However, warm inflation can happen when $Q_* > 1$ in multifield cases. For all cases we study in Fig. 5, n_s shows oscillatory features when Q_* changes, and this interesting feature also happens in Ref. [37].

We find $Q_* < 0.0018$, $r > 0.0090$ for $R_{\rm m} = 1$, which means only weak versions of warm inflation are allowed by observation, and this is consistent with the previous studies on single-field warm inflation [45]. When $R_{\rm m} = 1.5$, the dissipative strength Q_* can take values $Q_* < 0.0024$, and $r > 0.0077$. In case of $R_{\rm m} = 2$, Q_* lies in a slightly wider range $Q_* < 0.0044$, and r takes values $r > 0.0057$. For $R_{\rm m} = 3$, Q_* can be as large as 100, which means warm inflation is no longer restricted to weak regimes, and this is very different from single-field cases. In this case, r has a lower bound about 10^{-15}.

Another potential discriminator between different inflationary models is the non-Gaussianity produced during inflation. The nonlinear parameter $f_{\rm NL}$ is given by

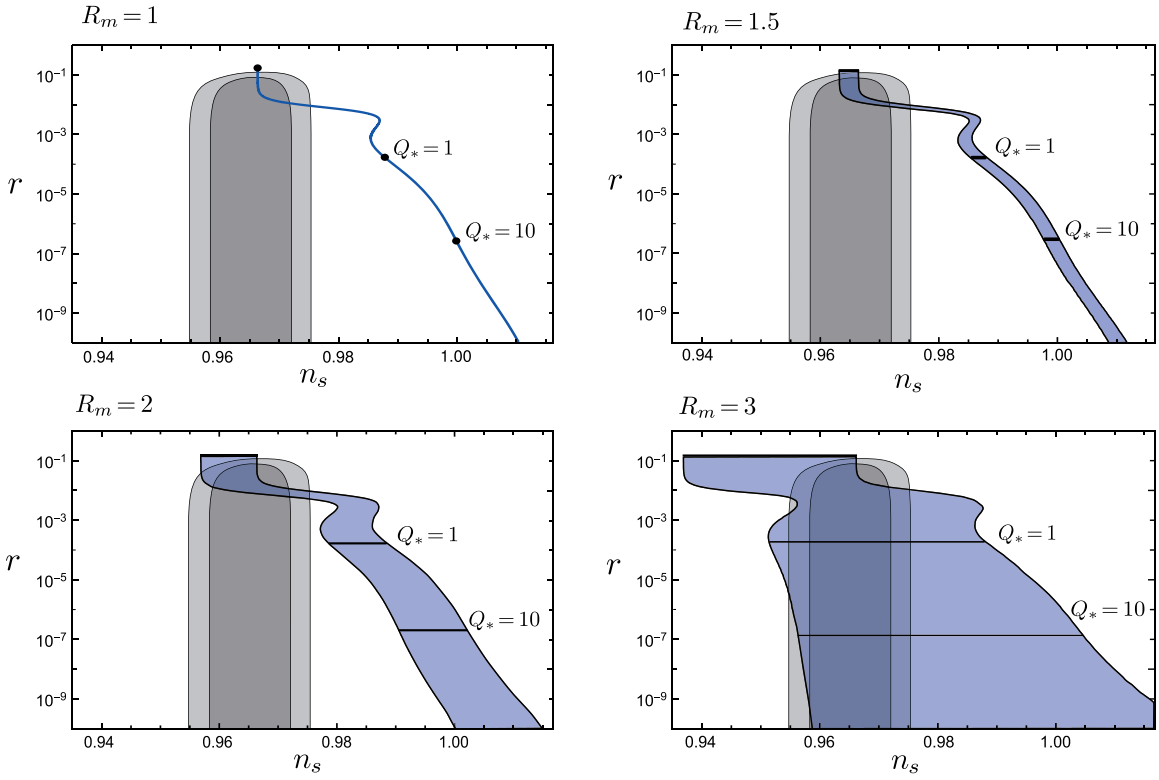

FIG. 5. Observational predictions (blue regions) of two-field warm inflation models with differential mass ratio $R_{\rm m}$. The gray contours correspond to the 68% and 95% C.L. results from Planck 2018 TT,TE,EE+lowE+lensing data. Note that when $R_{\rm m} = 1$ the results are the same as in the single-field case. The black lines at the top of blue regions in each panel denote $Q_* = 0$ (cold two-field inflation). The lower right panel shows that strong dissipative warm inflation is observationally favored due to the multifield effects in warm inflation.

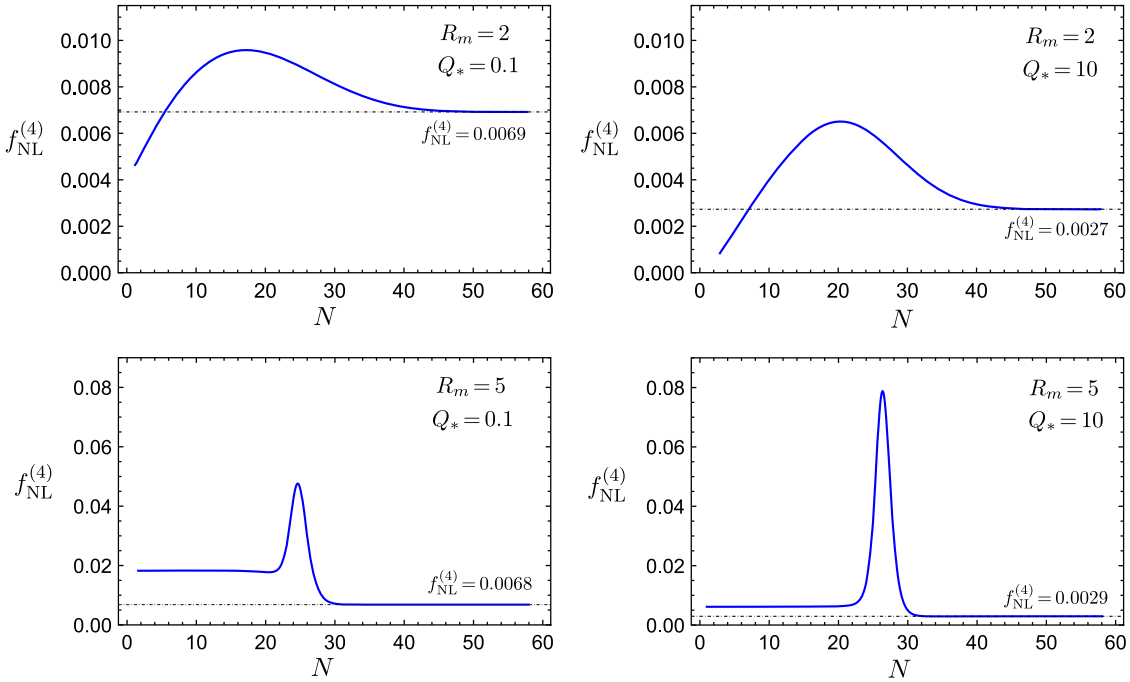

FIG. 6. The evolution of nonlinear parameter $f_{\rm NL}^{(4)}$. We take $R_m = 2, 5$ and $Q_* = 0.1, 10$, and the values of $f_{\rm NL}^{(4)}$ at the end of inflation are indicated in each panel. In our numerical examples, turns of the trajectories in field space all occur between $N = 10$ and $N = 30$.

$$f_{\rm NL} = f_{\rm NL}^{(3)} + f_{\rm NL}^{(4)}, \tag{4.4}$$

where $f_{\rm NL}^{(3)}$ is a slow-roll suppressed term coming from the intrinsic non-Gaussianity in $\delta\phi$ and $\delta\chi$. It has been shown that $f_{\rm NL}^{(3)}$ is much less than unity [46], which is too small to be observed by the current CMB experiment. Therefore, we will concentrate on the second term $f_{\rm NL}^{(4)}$, which can be expressed using the δN formalism [15],

$$f_{\rm NL}^{(4)} = \frac{5}{6}\frac{\sum_{IJ} N_{,IJ} N_{,I} N_{,J}}{(\sum_I N_{,I}^2)^2}, \tag{4.5}$$

where $N_{,I} = \partial N/(\partial\varphi_*^I)$, $N_{,IJ} = \partial^2 N/(\partial\varphi_*^I \partial\varphi_*^J)$, and the indices I and J run over all of the fields.

We have performed some numerical calculations of $f_{\rm NL}^{(4)}$ using Eq. (4.5) and obtained the final value of $f_{\rm NL}^{(4)}$ at the end of inflation. According to our results, the nonlinear parameter $f_{\rm NL}^{(4)} = 2.3 \times 10^{-3}$ for strong dissipative warm inflation, and $f_{\rm NL}^{(4)} = 6.9 \times 10^{-3}$ for weak dissipative warm inflation. Our results are of the same order of magnitude as some previous studies on warm inflation and multifield inflation [13,20,47,48]. In Fig. 6, taking $R_{\rm m} = 2$, 5 and $Q_* = 0.1$, 10 as examples, we give the evolution of $f_{\rm NL}^{(4)}$ from the Hubble exit until the end of inflation. As illustrated in Fig. 6, $f_{\rm NL}^{(4)}$ grows sharply when the heavy field decays to zero, corresponding to the turn of the trajectory in field space, but then decreases. After this moment, there is only one effective field, and the nonlinear parameter becomes slow-roll suppressed, which is the same as in single-field inflation. We can also conclude from Fig. 6 that multifield inflation does not necessarily produce large non-Gaussianity, and the mass ratio R_m does not have a significant impact on the final nonlinear parameter $f_{\rm NL}^{(4)}$.

V. CONCLUSIONS

In this work, we have tried to explore the main features of perturbations in two-field warm inflation and then use the observational data to constrain our models. We use the two-field quadratic warm inflation model with a linear-T dissipative coefficient as a representative example and carry out exhaustive numerical simulations to reveal the main features of multifield warm inflation. First, we derived the full set of equations describing background dynamics and perturbations. Taking into account the stochastic noise, these is a set of coupled stochastic differential equations (SDEs). Then we apply the formula to an example and get the main features of the evolution of perturbations by solving the SDEs numerically. We have shown that the curvature perturbation $\mathcal{R} \approx \mathcal{R}_\sigma \approx \mathcal{R}_r$ in superhorizon scales and the isocurvature will decay to zero before the end of inflation. In the following calculation, instead of integrating the SDEs to the end of inflation directly, we take a less computationally intensive method to get the power spectrum at the end of inflation. We use a, analytic formula (2.17) to describe $\mathcal{P}_\mathcal{R}$ at horizon crossing, in which the growing function $G(Q_*)$ is obtained by a fully numerical method. After horizon crossing, δN formalism is used to get the final power spectrum $\mathcal{P}_\mathcal{R}$ at the end of inflation. With the observational constraints $\mathcal{P}_\mathcal{R} = 2.2 \times 10^{-9}$ and $N_e = 60$, we obtain a set of (n_s, r) for every initial condition (ϕ_*, χ_*), as illustrated in Fig. 4. At last, we show our results in the (n_s, r) plane in Fig. 5 and compare the observational predictions of our models with the latest Planck data.

According to Fig. 5, we know that in single-field inflation warm inflation only occurs in the weak dissipative regime because the strong dissipation will render the power spectrum blue tilted, which is not compatible with observation. However, the multifield effects will cause the spectral index n_s to take values in a wide range for every r, rather than just a point. In this condition, observations are less effective in constraining n_s, and when the multifield effects are large enough, strong versions of warm inflation can become favored by observation.

The thick black line in each panel of Fig. 5 represents $Q_* = 0$ (cold inflation), from which we know the multi- effects will not change the tensor-to-scalar ratio r very much. Therefore, the inflationary models ruled out by observation for predicting too large r may not be rescued in the multifield case.

The existence of isocurvature perturbations will lead to the time evolution of the curvature perturbation $\mathcal{R}$, and this evolution can happen even in the postinflationary era. Therefore, multifield inflation is generally not predictive, unless an adiabatic limit is reached before the end of inflation. Fortunately, in all the cases we studied, the isocurvature mode of perturbations decays to zero before the end of inflation, as illustrated in Fig. 2. However, Fig. 5 shows even in this condition two-field warm inflation models are not well constrained by the observational results of (n_s, r), especially when the mass ratio $R_{\rm m}$ is large. In this case, other observational predictions such as the running of the spectral index can be used to constrain inflationary models, and we will leave this to future study. On the other hand, if two mass scales are widely separated, inflation tends to be dominated by only the light field. Under this circumstance, we will go back to single-field warm inflation.

Compared with single-field cases, slow-roll parameters may become relatively large in multifield warm inflation. We have to go beyond the slow-roll approximations, or some important features will be lost. Figure 2 shows that the slow-roll parameters ϵ and η have local extremes when the heavy field χ decays to zero, and this effect becomes more obvious when the mass ratio $R_{\rm m}$ is large. If these extremes occur at horizon crossing by coincidence, the slow-roll corrections will make the analytic expression (2.17) less

accurate in describing the power spectrum at horizon crossing. As demonstrated by Fig. 3, larger $R_{\rm m}$ will lead to higher residuals when we use the grow function $G(Q_*)$ to fit the data obtained by numerical simulation. A possible way to deal with this problem is that we can integrate the stochastic perturbation equations (2.18), (2.19), and (2.20) directly to the end of inflation without introducing the analytic formula (2.17) at horizon crossing, which is a more computationally extensive method. From this work, we can conclude that even the simplest two-field warm inflation models are much more complicated than single-field cases, and this topic needs further investigations.

Note that in two-field quadratic warm inflation, when $m_\phi = m_\chi$, the background trajectory in field space is a straight line, regardless of the initial conditions. Therefore, the isocurvature mode of perturbation has no influence on curvature perturbation according to Eqs. (2.18)–(2.20), so the perturbation features are the same for the single-field case, as illustrated in the top left panel in Fig. 5. However, this property no longer exists in other two-field warm inflation models. For example, in two-field quartic inflation with a potential $V = \frac{1}{4}\lambda_\phi\phi^4 + \frac{1}{4}\lambda_\chi\chi^4$, the $\lambda_\phi = \lambda_\chi$ case is not equivalent to single-field inflation (we describe more details in Appendix B). Besides, the dissipative coefficient γ can be different for ϕ and χ in general. In this work, we use a common γ just for simplicity, and this topic needs further study.

ACKNOWLEDGMENTS

This work was supported by the National Natural Science Foundation of China (Grants No. 11575270, No. 11175019, No. 11235003, and No. 11605100).

APPENDIX A: PERTURBATION EQUATIONS IN MULTIFIELD WARM INFLATION

In this section, we will present some perturbation equations in multifield warm inflation. For a multicomponent system consisting of two scalar fields φ_I $(I = 1, 2)$ and a radiation fluid, the Einstein equation of the system is given by [49]

$$G_{\mu\nu} = T^{(\varphi)}_{\mu\nu} + T^{(r)}_{\mu\nu}, \tag{A1}$$

where

$$T^{(\varphi)}_{\mu\nu} = \Sigma_I \partial_\mu\varphi_I\partial_\nu\varphi_I - g_{\mu\nu}\left(\frac{1}{2}\Sigma_I\partial^\lambda\varphi_I\partial_\lambda\varphi_I + V(\varphi)\right), \tag{A2}$$

$$T^{(r)}_{\mu\nu} = (\rho_r + p_r)u_\mu u_\nu + p_r g_{\mu\nu}, \tag{A3}$$

where $G_{\mu\nu}$ is the Einstein tensor and $T^{(\varphi)}_{\mu\nu}$ and $T^{(r)}_{\mu\nu}$ are the energy-momentum tensor of scalar fields and radiation fluid. For the radiation fluid, $p_r = \frac{1}{3}\rho_r$, $\delta p_r = \frac{1}{3}\delta\rho_r$, where p_r and ρ_r are the pressure and energy density of the radiation and δp_r and $\delta\rho_r$ are their perturbations, respectively.

For simplicity, we will work in the spatially flat gauge $(E = \psi = 0)$. According to the perturbation equations of the Einstein equation, we can represent metric perturbations A and B in terms of perturbations of scalar fields and radiation [50],

$$A = \frac{-\delta q_r + \Sigma_I\dot{\varphi_I}\delta\varphi_I}{2H}, \tag{A4}$$

$$\begin{aligned} B = &-\frac{a}{4k^2H^2}(24H^2\delta q_r \\ &+ (4\rho_r + \Sigma_I\dot{\varphi_I}^2)(-\delta q_r + \Sigma_I\dot{\varphi_I}\delta\varphi_I) \\ &+ 2H(3\delta\dot{q_r} + 4\gamma\Sigma_I\dot{\varphi_I}\delta\varphi_I + \Sigma_I\ddot{\varphi_I}\delta\varphi_I - \Sigma_I\dot{\varphi_I}\,\delta\dot{\varphi_I})), \end{aligned} \tag{A5}$$

where $\delta q_r = a(p_r + \rho_r)(B + \delta u)$ is the momentum density perturbation of radiation. The variation of the scalar field's equation of motion is given by [51]

$$\begin{aligned} &\delta\ddot{\varphi}_I + (3H + \gamma)\delta\dot{\varphi}_I + \frac{k^2}{a^2}\delta\varphi_I + \Sigma_J V_{\varphi_I\varphi_J}\delta\varphi_J + \dot{\varphi_I}\delta\gamma \\ &\quad = -(2V_{\varphi_I} + \gamma\dot{\varphi_I})A + \dot{\varphi_I}\left(\dot{A} - \frac{k^2}{a}B\right). \end{aligned} \tag{A6}$$

After some adaption, the perturbation of energy and momentum conservation equations of the radiation leads to [18,52]

$$\begin{aligned} &\delta\ddot{q}_r + 7H\delta\dot{q}_r + 3\left(7H^2 + \dot{H} + \frac{1}{3}\frac{k^2}{a^2}\right)\delta q_r \\ &\quad + \Sigma_I\left(\frac{1}{3}\dot{\varphi_I}^2\delta\gamma + (4H\gamma + \dot{\gamma})\dot{\varphi_I}\delta\varphi_I + \gamma\ddot{\varphi_I}\delta\varphi_I + \frac{5}{3}\gamma\dot{\varphi_I}\,\delta\dot{\varphi_I}\right) \\ &= \frac{1}{3}\frac{k^2}{a}\rho_r B - \frac{16}{3}H\rho_r A + \frac{1}{3}\gamma\Sigma_I\dot{\varphi_I}^2 A - \frac{4}{3}\rho_r\dot{A}. \end{aligned} \tag{A7}$$

Substituting Eqs. (2.7) and (2.10) into Eqs. (A6) and (A7), we can get

$$\begin{aligned} &\delta\ddot{\sigma} + (3H + \gamma)\delta\dot{\sigma} + \left(\frac{k^2}{a^2} + V_{\sigma\sigma} - \dot{\theta}^2\right)\delta\sigma - 2\dot{\theta}\,\delta\dot{s} \\ &\quad + 2\left(\frac{2\dot{\theta}V_\sigma}{\dot{\sigma}} - \ddot{\theta}\right)\delta s + \dot{\sigma}\delta\gamma \\ &\quad = -\frac{k^2}{a}\dot{\sigma}B - (\dot{\sigma}\gamma + 2V_\sigma)A + \dot{\sigma}\,\dot{A}, \end{aligned} \tag{A8}$$

$$\delta\ddot{s}+(3H+\gamma)\delta\dot{s}+\left(\frac{k^2}{a^2}+V_{ss}-\dot{\theta}^2\right)\delta s+2\dot{\theta}\,\delta\dot{\sigma}-\frac{2\dot{\theta}\,\ddot{\sigma}}{\dot{\sigma}}\delta\sigma=2\dot{\theta}\,\dot{\sigma}\,A, \tag{A9}$$

$$\delta\ddot{q}_r+7H\delta\dot{q}_r+3\left(7H^2+\dot{H}+\frac{1}{3}\frac{k^2}{a^2}\right)\delta q_r+\frac{5}{3}\gamma\dot{\sigma}\,\delta\dot{\sigma}+(\gamma\ddot{\sigma}+\dot{\gamma}\,\dot{\sigma}+4H\gamma\dot{\sigma})\delta\sigma+\frac{1}{3}\dot{\sigma}^2\delta\gamma-\frac{2}{3}\gamma\dot{\theta}\,\dot{\sigma}\,\delta s=\frac{1}{3}\frac{k^2}{a}\rho_r B-\frac{16}{3}H\rho_r A+\frac{1}{3}\gamma\dot{\sigma}^2 A-\frac{4}{3}\rho_r\dot{A}, \tag{A10}$$

Note that in the case of $\gamma=C_T T$ we have $\delta\gamma/\gamma=\delta T/T=\delta\rho_r/(4\rho_r)$, and $\delta\gamma$ has been eliminated from perturbation equations. Taking into account the stochastic noise ξ and changing the time variable from cosmic time t to e-foldings N, we can obtain the perturbation equations in Sec. II.

APPENDIX B: TWO-FIELD QUADRATIC INFLATION WITH EQUAL MASSES

According to background equations (2.22) and (2.23), in the case of $m_\phi=m_\chi=m$, for two-field quadratic inflation, we have

$$\phi''+(3+3Q-\epsilon)\phi'+m^2\phi/H^2=0, \tag{B1}$$

$$\chi''+(3+3Q-\epsilon)\chi'+m^2\chi/H^2=0. \tag{B2}$$

where

$$V_{\sigma\sigma}=\cos^2\theta V_{\phi\phi}+\sin 2\theta V_{\phi\chi}+\sin^2\theta V_{\chi\chi}, \tag{A11}$$

$$V_{ss}=\sin^2\theta V_{\phi\phi}-\sin 2\theta V_{\phi\chi}+\cos^2\theta V_{\chi\chi}. \tag{A12}$$

Substituting Eqs. (A4) and (A5) into Eqs. (A8)–(A10) and expressing the equations in terms of $\mathcal{R}_\sigma$ and $\mathcal{R}_r$ using $\mathcal{R}_\sigma=H\delta\sigma/\dot{\sigma}$, $\mathcal{R}_r=-H\delta q_r/(p_r+\rho_r)$, we get

$$\ddot{\mathcal{R}}_\sigma+\left(3H+\gamma+\frac{4\rho_r}{3H}+\frac{\dot{\sigma}^2}{H}+\frac{2\ddot{\sigma}}{\dot{\sigma}}\right)\dot{\mathcal{R}}_\sigma+\left(\frac{k^2}{a^2}+H\gamma-\dot{\theta}^2+\frac{4\rho_r}{3}+\frac{2\gamma\rho_r}{3H}+\frac{8{\rho_r}^2}{9H^2}-\frac{11\gamma\dot{\sigma}^2}{6H}-\frac{\gamma^2\dot{\sigma}^2}{\rho_r}+\frac{4\rho_r\ddot{\sigma}}{3H\dot{\sigma}}\right)\mathcal{R}_\sigma$$
$$=-\left(\gamma+\frac{4\rho_r}{3H}\right)\dot{\mathcal{R}}_r+\left(H\gamma+\frac{4\rho_r}{3}+\frac{2\gamma\rho_r}{3H}+\frac{8{\rho_r}^2}{9H^2}-\frac{11\gamma\dot{\sigma}^2}{6H}-\frac{\gamma^2\dot{\sigma}^2}{\rho_r}+\frac{4\rho_r\ddot{\sigma}}{3H\dot{\sigma}}\right)\mathcal{R}_r+\frac{2H\dot{\theta}}{\dot{\sigma}}\delta\dot{s}+\left(\frac{6H^2\dot{\theta}}{\dot{\sigma}}+\frac{2H\gamma\dot{\theta}}{\dot{\sigma}}+\frac{2H\ddot{\theta}}{\dot{\sigma}}+\dot{\theta}\,\dot{\sigma}+\frac{2H\dot{\theta}\,\ddot{\sigma}}{\dot{\sigma}^2}\right)\delta s, \tag{A13}$$

$$\ddot{\mathcal{R}}_r+\left(-H+\frac{4\rho_r}{3H}+\frac{\dot{\sigma}^2}{H}+\frac{7\gamma\dot{\sigma}^2}{4\rho_r}\right)\dot{\mathcal{R}}_r+\left(\frac{k^2}{3a^2}+\frac{3\gamma\dot{\sigma}^2}{2H}+\frac{9H\gamma\dot{\sigma}^2}{4\rho_r}+\frac{8\rho_r\dot{\sigma}^2}{9H^2}+\frac{\dot{\sigma}^4}{2H^2}+\frac{7\gamma\dot{\sigma}^4}{8H\rho_r}+\frac{\dot{\sigma}\,\ddot{\sigma}}{H}+\frac{2\gamma\dot{\sigma}\,\ddot{\sigma}}{\rho_r}\right)\mathcal{R}_r$$
$$=\left(\frac{\dot{\sigma}^2}{3H}+\frac{5\gamma\dot{\sigma}^2}{4\rho_r}\right)\dot{\mathcal{R}}_\sigma+\left(\frac{3\gamma\dot{\sigma}^2}{2H}+\frac{9H\gamma\dot{\sigma}^2}{4\rho_r}+\frac{8\rho_r\dot{\sigma}^2}{9H^2}+\frac{\dot{\sigma}^4}{2H^2}+\frac{7\gamma\dot{\sigma}^4}{8H\rho_r}+\frac{\dot{\sigma}\,\ddot{\sigma}}{H}+\frac{2\gamma\dot{\sigma}\,\ddot{\sigma}}{\rho_r}\right)\mathcal{R}_\sigma+\left(-\frac{1}{3}\dot{\theta}\,\dot{\sigma}+\frac{H\gamma\dot{\theta}\,\dot{\sigma}}{2\rho_r}\right)\delta s, \tag{A14}$$

$$\delta\ddot{s}+(3H+\gamma)\delta\dot{s}+\left(\frac{k^2}{a^2}-\dot{\theta}^2+V_{ss}\right)\delta s=-\frac{2\dot{\theta}\,\dot{\sigma}}{H}\dot{\mathcal{R}}_\sigma-\frac{4\dot{\theta}\,\dot{\sigma}\,\rho_r}{3H^2}\mathcal{R}_\sigma+\frac{4\dot{\theta}\,\dot{\sigma}\,\rho_r}{3H^2}\mathcal{R}_r. \tag{A15}$$

After some adaption, the above equations can be put in the form

$$(\phi'\chi-\chi'\phi)'+(3+3Q-\epsilon)(\phi'\chi-\chi'\phi)=0. \tag{B3}$$

The solution of the above equation is given by

$$(\phi'\chi-\chi'\phi)=Ce^{-\int_0^N(3+3Q-\epsilon)dN}, \tag{B4}$$

where C is an integration constant. During inflation, $Q>0$, and $\epsilon<1$; therefore,

$$|\phi'\chi-\chi'\phi|<|C|e^{-\int_0^N 2dN}=|C|e^{-2N}. \tag{B5}$$

From Eq. (B5), we know $\phi'\chi-\chi'\phi$ will tend to zero rapidly. When $(\phi/\chi)'=(\phi'\chi-\chi'\phi)/\chi^2\sim 0$, the trajectory

in field space will become a straight line, which is the same as the single-field case.

However, for two-field quartic inflation $V = \frac{1}{4}\lambda_\phi\phi^4 + \frac{1}{4}\lambda_\chi\chi^4$, the effective masses $m_\phi = V_{\phi\phi}$ and $m_\chi = V_{\chi\chi}$ are not constants during inflation, and in general, Eq. (B3) is not valid even for $\lambda_\phi = \lambda_\chi$. In this case, we cannot reach the above conclusion, and the background dynamics of two-field quartic inflation display more complex behavior.

[1] A. H. Guth, Inflationary universe: A possible solution to the horizon and flatness problems, Phys. Rev. D **23**, 347 (1981).
[2] A. D. Linde, A new inflationary universe scenario: A possible solution of the horizon, flatness, homogeneity, isotropy and primordial monopole problems, Phys. Lett. B **108**, 389 (1982).
[3] J. Yokoyama and K. Maeda, On the dynamics of the power law inflation due to an exponential potential, Phys. Lett. B **207**, 31 (1988).
[4] A. Berera, I. G. Moss, and R. O. Ramos, Warm inflation and its microphysical basis, Rep. Prog. Phys. **72**, 026901 (2009).
[5] X. B. Li, Y. Y. Wang, H. Wang, and J. Y. Zhu, Dynamic analysis of noncanonical warm inflation, Phys. Rev. D **98**, 043510 (2018).
[6] M. Bastero-Gil, A. Berera, R. O. Ramos, and J. G. Rosa, Adiabatic out-of-equilibrium solutions to the Boltzmann equation in warm inflation, J. High Energy Phys. 02 (2018) 063.
[7] X. M. Zhang and J. Y. Zhu, Consistency of the tachyon warm inflationary universe models, J. Cosmol. Astropart. Phys. 02 (2014) 005.
[8] A. Berera, J. Mabillard, M. Pieroni, and R. O. Ramos, Identifying universality in warm inflation, J. Cosmol. Astropart. Phys. 07 (2018) 021.
[9] J. Yokoyama and A. Linde, Is warm inflation possible?, Phys. Rev. D **60**, 083509 (1999).
[10] M. Bastero-Gil, A. Berera, R. O. Ramos, and J. G. Rosa, Warm Little Inflaton, Phys. Rev. Lett. **117**, 151301 (2016).
[11] Z. Lalak, D. Langlois, S. Pokorski, and K. Turzyński, Curvature and isocurvature perturbations in two-field inflation, J. Cosmol. Astropart. Phys. 07 (2007) 014.
[12] S. Weinberg, *Cosmology* (Oxford University, Oxford, 2008).
[13] F. Vernizzi and D. Wands, Non-Gaussianities in two-field inflation, J. Cosmol. Astropart. Phys. 05 (2006) 019.
[14] X. M. Zhang and J. Y. Zhu, Primordial non-Gaussianity in noncanonical warm inflation, Phys. Rev. D **91**, 063510 (2015).
[15] R. de Putter, J. Gleyzes, and O. Doré, The next non-Gaussianity frontier: What can a measurement with $\sigma(f_{\rm NL}) \lesssim 1$ tell us about multifield inflation? Phys. Rev. D **95**, 123507 (2017).
[16] I. Huston and A. J. Christopherson, Calculating nonadiabatic pressure perturbations during multifield inflation, Phys. Rev. D **85**, 063507 (2012).
[17] S. Renaux-Petel and K. Turzyński, On reaching the adiabatic limit in multi-field inflation, J. Cosmol. Astropart. Phys. 06 (2015) 010.
[18] Y. Y. Wang, J. Y. Zhu, and X. M. Zhang, Two-field warm inflation and its scalar perturbations on large scales, Phys. Rev. D **97**, 063510 (2018).
[19] C. Gordon, D. Wands, B. A. Bassett, and R. Maartens, Adiabatic and entropy perturbations from inflation, Phys. Rev. D **63**, 023506 (2000).
[20] K. Y. Choi, L. M. H. Hall, and C. van de Bruck, Spectral running and non-Gaussianity from slow-roll inflation in generalized two-field models, J. Cosmol. Astropart. Phys. 02 (2007) 029.
[21] S. Tsujikawa, D. Parkinson, and B. A. Bassett, Correlation-consistency cartography of the double-inflation landscape, Phys. Rev. D **67**, 083516 (2003).
[22] R. Kabir and A. Mukherjee, Oscillatory power spectrum and strongly k-dependent r in hybrid inflation, arXiv:1602.01221.
[23] K. A. Malik and D. Wands, Adiabatic and entropy perturbations with interacting fluids and fields, J. Cosmol. Astropart. Phys. 02 (2005) 007.
[24] K. A. Malik, Cosmological perturbations in an inflationary universe, arXiv:astro-ph/0101563.
[25] S. Cespedes, V. Atal, and G. A. Palma, On the importance of heavy fields during inflation, J. Cosmol. Astropart. Phys. 05 (2012) 008.
[26] I. G. Moss and C. Xiong, Non-Gaussianity in fluctuations from warm inflation, J. Cosmol. Astropart. Phys. 04 (2007) 007.
[27] L. M. H. Hall and I. G. Moss, Scalar perturbation spectra from warm inflation, Phys. Rev. D **69**, 083525 (2004).
[28] W. L. Lee and L. Z. Fang, A relativistic calculation of super-Hubble suppression of inflation with thermal dissipation, Classical Quantum Gravity **17**, 4467 (2000).
[29] C. Graham and I. G. Moss, Density fluctuations from warm inflation, J. Cosmol. Astropart. Phys. 07 (2009) 013.
[30] N. Videla and G. Panotopoulos, Observational constraints on warm quasi-exponential inflation, Phys. Rev. D **97**, 123503 (2018).
[31] L. Visinelli, Observational constraints on monomial warm inflation, J. Cosmol. Astropart. Phys. 07 (2016) 054.
[32] M. Bastero-Gil, A. Berera, and R. O. Ramos, Shear viscous effects on the primordial power spectrum from warm inflation, J. Cosmol. Astropart. Phys. 07 (2011) 030.
[33] A. R. Liddle and D. H. Lyth, *Cosmological Inflation and Large-Scale Structure* (Cambridge University Press, Cambridge, England, 2000).
[34] R. O. Ramos and L. A. da Silva, Power spectrum for inflation models with quantum and thermal noises, J. Cosmol. Astropart. Phys. 03 (2013) 032.

[35] T. Matsuda, Evolution of the curvature perturbations during warm inflation, J. Cosmol. Astropart. Phys. 06 (2009) 002.
[36] M. Bastero-Gil, A. Berera, and N. Kronberg, Exploring the parameter space of warm-inflation models, J. Cosmol. Astropart. Phys. 12 (2015) 046.
[37] M. Bastero-Gil, S. Bhattacharya, K. Dutta, and M. R. Gangopadhyay, Constraining warm inflation with CMB data, J. Cosmol. Astropart. Phys. 02 (2018) 054.
[38] M. Bastero-Gil, A. Berera, R. Hernández-Jiménez, and J. G. Rosa, Dynamical and observational constraints on the warm little inflaton scenario, Phys. Rev. D **98**, 083502 (2018).
[39] B. Feng and X. Zhang, Double inflation and the low CMB quadrupole, Phys. Lett. B **570**, 145 (2003).
[40] K. Li, X. M. Zhang, H. Y. Ma, and J. Y. Zhu, Noncanonical warm inflation: A model with a general Lagrangian density, Phys. Rev. D **98**, 123528 (2018).
[41] M. Bastero-Gil, A. Berera, I. G. Moss, and R. O. Ramos, Cosmological fluctuations of a random field and radiation fluid, J. Cosmol. Astropart. Phys. 05 (2014) 004.
[42] M. Dias, J. Frazer, and D. Seery, Computing observables in curved multifield models of inflation—A guide (with code) to the transport method, J. Cosmol. Astropart. Phys. 12 (2015) 030.
[43] A. Riotto, Inflation and the theory of cosmological perturbations, arXiv:hep-ph/0210162.
[44] Y. Akrami *et al.* (Planck Collaboration), Planck 2018 results. X. Constraints on inflation, arXiv:1807.06211.
[45] M. Benetti and R. O. Ramos, Warm inflation dissipative effects: Predictions and constraints from the Planck data, Phys. Rev. D **95**, 023517 (2017).
[46] D. H. Lyth and I. Zaballa, A bound concerning primordial non-Gaussianity, J. Cosmol. Astropart. Phys. 10 (2005) 005.
[47] S. Gupta, Dynamics and non-Gaussianity in the weak-dissipative warm inflation scenario, Phys. Rev. D **73**, 083514 (2006).
[48] D. Battefeld and T. Battefeld, Non-Gaussianities in N-flation, J. Cosmol. Astropart. Phys. 05 (2007) 012.
[49] Z. P. Peng, J. N. Yu, X. M. Zhang, and J. Y. Zhu, Perturbation spectra in the warm k-inflation, Phys. Rev. D **97**, 063523 (2018).
[50] N. Bartolo, P. Corasaniti, A. Liddle, and M. Malquarti, Perturbations in cosmologies with a scalar field and a perfect fluid, Phys. Rev. D **70**, 043532 (2004).
[51] I. Huston and A. J. Christopherson, Isocurvature perturbations and reheating in multi-field inflation, arXiv:1302.4298.
[52] C. Pitrou, X. Roy, and O. Umeh, xPand: An algorithm for perturbing homogeneous cosmologies, Classical Quantum Gravity **30**, 165002 (2013).